PERGAMON

International Journal of Heat and Mass Transfer 45 (2002) 619–630

International Journal of HEAT and MASS TRANSFER

www.elsevier.com/locate/ijhmt

3-D finite element simulation of wafer thermal distortion and stress fields in exposure process

Zone-Ching Lin [a,*], Wen-Jang Wu [b]

[a] Department of Mechanical Engineering, National Taiwan University of Science and Technology, 43 Keelung Road, Section 4, Taipei 10672, Taiwan, ROC

[b] Department of Mechanical Engineering, National Lien-Ho Institute of Technology, Miao-Li, Taiwan, ROC

Received 3 November 2000; received in revised form 6 April 2001

Abstract

A 3-D thermo-elastic finite element model was established in this paper to study the transient behavior of thermal expansion and the distribution of thermal stress in a wafer by the absorption of exposure energy during the exposure process. The analysis procedure of investigating the thermal expansion of the wafer including the transient behavior in a single exposure region, the thermal interactions between neighboring exposure regions to the variation of exposure energy, the interval of exposure locations, and ends with the interval of exposure time under continuous exposure. The results indicate that the thermal deformation gradient of the wafer can be improved by adjusting the location interval and the time interval between the neighboring exposure regions. Widening the interval of exposure locations has a greater impact in improving the thermal deformation of wafer than extending the interval of exposure time between the image fields. The physical phenomenon can serve as a supporting reference tool for engineers in planning exposure paths, and the simulation model can serve as an analysis tool to understand the behavior during the exposure process. © 2001 Elsevier Science Ltd. All rights reserved.

Keywords: Exposure; Finite element method; Wafer; Thermal deformation; Thermal stress

1. Introduction

As the wafer diameter increases over time and the circuit line width continues to shrink, certain process problems previously overlooked must now be taken into consideration. For example, during the exposure process of photolithography, the exposure energy absorbed by the wafer causes the wafer temperature to rise and produce expansion. This phenomenon was often overlooked in the previous generation of litho graphic processes due to their limited effect. However, in the new generation of litho graphic processes, it may well become a very important factor. This type of local temperature increase causes a discrepancy between the height at the location of the exposure field center and that at the expanded edge region. This discrepancy results in inconsistency in the depth of focus when the pattern on mask is projected onto the wafer surface. In addition, deformation from horizontal thermal expansion produces overlay error.

Saito [1] point out that the cause of the scaling error is proved to be local wafer expansion due to the accumulated heat generated by the exposure light energy. His experiment shown that, under high-energy exposure, the distribution of overlay error is related to the path of exposure scan. This is because wafer absorbed different amounts of exposure energy at different locations. The resulting difference in temperature increase caused uneven thermal expansion, which produced irregular scaling error in the circuit pattern. His simulation analysis adopted a fixed path of exposure, but ignored the heat transfer effect of the wafer stage and replaced it simply by the boundary heat transmission.

In their paper of Gegenwarth and Laming [2], the stored stress left after the sawing and lapping of a silicon

* Corresponding author. Tel.: +886-2737-6455; fax: +886-2737-6429.

E-mail address: zclin@mail.ntust.edu.tw (Z.-C. Lin).

0017-9310/02/$ - see front matter © 2001 Elsevier Science Ltd. All rights reserved.
PII: S0017-9310(01)00163-6

wafer could produce plastic flow and cause overlay error when the wafer temperature increased to 600°C. That is, the internal status of wafer changed as temperature increased. Yau [3] found that the process-induced distortion in silicon wafers, regardless of films grown on the wafer surface or deposited on wafer, results in different degrees of bow in the wafer along with changes in temperature due to different thermal expansion coefficients of the thin film and wafer substrate. Lau [4] studied the distribution of the wafer temperature produced by an uneven circular heat source to analyze the correlation between the distribution of temperature and variation in wafer thickness. Later on, Lau [5] further studied the distribution of wafer temperature produced by an even rectangular heat source. Haytcher and Engelstad [6] used the finite element method to simulate expansion deformation of patterns caused by rising temperature on the mask due to exposure to X-rays. Shen et al. [7] used the finite element methods to simulate variation of the wafer bow as a result of temperature increase when the circuit line width on the wafer surface changed. The simulation results indicated that, when the bottom of wafer was not subject to restrictions, the curvature increased as the wafer temperature rose. Lee and Mack [8] used finite element methods to simulate wafer processing and examine the correlation between temperature variation and stress distribution inside the wafer during different stages of the process. In addition, rapid thermal processing is a new technology in wafer processing [9–11]. How to control the wafer temperature to avoid the uneven thermal stress and deformation becomes a serious topic.

Most of researchers effort focuses on the analysis of the behavior and status of the entire wafer under high temperature and long period of processing. The emphasis of research is the plastic deformation or warpage. However, wafer absorbs exposure energy in a very short instant during the lithographic exposure process. Hence, there is only a remote possibility of plastic deformation. The exposure area represents only a very small part of the entire wafer at a time. Because the bottom of the wafer is clamped by vacuum chuck, the phenomenon of warpage is restricted. Thus, the behavior of the variation of wafer temperature during exposure is different from that in ordinary heating processes and only local changes on the wafer need to be considered. In this paper, the finite element model was used to establish a simulation program in order to study the expansion deformations and the thermal stress in the wafer under different exposure conditions.

2. Mathematical model

The ordinary transient heat transfer equation for a 3-D solid body is

$$\left(\frac{\partial}{\partial x}\left(k_x\frac{\partial T}{\partial x}\right)+\frac{\partial}{\partial y}\left(k_y\frac{\partial T}{\partial y}\right)+\frac{\partial}{\partial z}\left(k_z\frac{\partial T}{\partial z}\right)\right)+q=\rho c\frac{\partial T}{\partial t}, \tag{1}$$

where T is the material temperature, q is the internal heat generation rate per unit volume, ρ is the material density, c is the specific heat, t is the time, k_x, k_y and k_z denote the thermal conductivity coefficients of the solid body in three axial directions, respectively. Let the weighting function equal the shape function. Then, the heat transfer finite element model can be obtained by means of the Galerkin method [12]:

$$[K_\theta]\{\theta\}+[K_c]\left\{\frac{\partial\{\theta\}}{\partial t}\right\}=\{F_t\}, \tag{2}$$

where $\{\theta\}$ is the temperature of element node, $[K_\theta]$ is the stiffness matrix for heat transfer, $[K_c]$ is the capacitance matrix and $\{F_t\}$ is the temperature load matrix.

If the body force of various nodes is ignored, the thermal-elastic finite element equation can be inferred based on the principle of minimum potential energy [12]

$$[K_d]\{d\}=\{F_d\}, \tag{3}$$

where $\{d\}$ is the element's nodal displacement, $[K_d]$ is the stiff matrix of elastic elements and $\{F_d\}$ is the resultant of loads of the node. Then the relation between element stress and nodal displacement can be written as

$$\{\sigma\}=[D^e]([B_d]\{d\}-\{\varepsilon^t\}), \tag{4}$$

where $\{\varepsilon^t\}$ is the nodal initial force vector caused by the thermal strain, $[D^e]$ is the elastic stiffness matrix and $[B_d]$ is the strain–displacement relation matrix.

For the sake of comparing the distribution of stress of various nodes, the stress status of all nodes can be expressed by means of an equivalent stress, σ_e

$$\sigma_e=\sqrt{\frac{(\sigma_{xx}-\sigma_{yy})^2+(\sigma_{yy}-\sigma_{zz})^2+(\sigma_{zz}-\sigma_{xx})^2+6(\sigma_{xy}^2+\sigma_{yz}^2+\sigma_{zx}^2)}{2}}. \tag{5}$$

3. Assumptions of simulation conditions

When the optical heating energy enters a wafer, as shown in Fig. 1(a), most of the exposure energy absorbed by the wafer. Part of the energy is transferred to the stage in contact with the wafer through heat transfer. The wafer is clamped to the stage by a vacuum chuck to prevent wafer sliding during the advancement and exposure. Since the thickness of wafer is often smaller than 1 mm and the height of stage often exceeds 10 mm, there is a tremendous difference in thickness. The wafer volume is also far smaller than that of the stage. Thus, the simulated wafer exposure mechanism in this paper, as shown in Fig. 1(b),

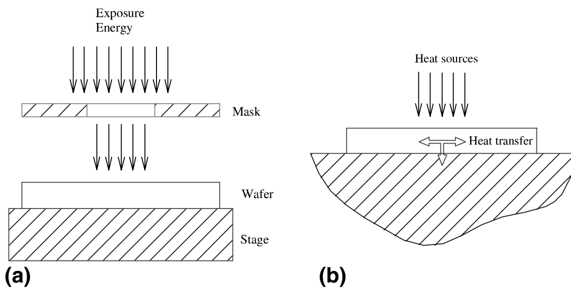

Fig. 1. Mechanism of wafer exposure: (a) mechanism of wafer exposure; (b) simplified simulation of mechanism.

assumes the stage thickness to be infinitely large for simplify the model.

3.1. Grid division and assumptions of boundary conditions

The model of grid division and boundary conditions adopted is shown in Fig. 2. As shown in Fig. 2(a), the division is done by equal intervals. The wafer is divided into combinations of hexahedron elements. Each of elements further divided into five constant strain tetrahedron elements to serve as the smallest unit for finite element analysis. The advantage of this Cartesian coordinate mesh division is that all exposure fields and chips take the shape of a square. This makes it more convenient in processing the exposure heat source and pattern deformation in the image field. Of course, the wafer edge produced by such element division method is not really an arch shape. Fortunately, the locations of exposure during simulation are all near the center of wafer. The unilateral length of exposure area is far smaller than the wafer radius. With very short periods of exposure time, the amount of thermal energy transferred to the wafer edge is very limited and the edge effects are very small. Thus, the element division method in this study should be acceptable. During continuous exposure, the center point of the image field falls right on the X-axis in simulation. Beside, the distribution of wafer temperature and deformation are both symmetrical to the X-axis. It is thus only necessary to simulate half of the wafer.

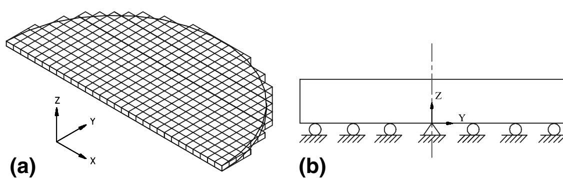

Fig. 2. Element division model and assumptions of deformation boundary conditions: (a) element division model; (b) boundary conditions.

It is assumed that the contact boundary condition between a wafer and the wafer stage is a roller support as shown in Fig. 2(b). The wafer stage is fixed and the deformation of a wafer is only in the Y- and X-directions in this paper. This assumption is correct, because the deformation of the stage is ignored in this paper. It is also assumed that the contact surface between wafer and stage is clamped by vacuum chuck and the warpage of the wafer can be ignored. At the contact surface between the wafer and the stage, i.e. $Z = 0$, the wafer can expand freely along the X–Y plane, but cannot leave the stage surface. In Fig. 2(b), roller support denotes freely sliding expansion and since the exposure path falls on the X-axis, the wafer deformation is symmetrical to the X-axis. Hence, when $Y = 0$, fixed support is shown in the figure to denote restriction to wafer expansion deformation. If expressed in mathematical equations, the combination of the boundary conditions of wafer deformation is written as:

$$d_{iy} = 0 \quad \text{at } Y = 0, \tag{6}$$

$$d_{iz} = 0 \quad \text{at } Z = 0, \text{ and} \tag{7}$$

$$f_{iz} = 0 \quad \text{at } Z \neq 0, \tag{8}$$

where d_{iy} is the displacement of the ith node in the Y-axis direction, d_{iz} is the displacement of the ith node in the Z-axis direction and f_{iz} is the nodal force of the ith node in the Z-axis direction.

Since the yellow room where wafer exposure takes place has extremely strict control on airflow to prevent pollution from airborne particles, the effect of air convection on wafer exposure is extremely limited. Hence, the effect of air thermal convection is ignored in the heat transfer boundary conditions adopted in our simulation. In the finite element model for heat transfer, as written in Eq. (2), the internally produced temperature load is absent from our simulation model. Thus, the primary temperature load comes from the external heat load on the wafer boundary.

There are three possibilities for the composition of the boundary temperature load matrix $\{F_t\}$:

(1) *Elements on the wafer upper surface within the exposure region*. They are subjected to the external exposure energy, q_e, and the heat load produced is

$$\{F_t\} = \int\int_A q_e\{N\}\,dA, \tag{9}$$

where q_e is 500 mw/cm^2, $\{N\}$ is the shape function and A is the area of the element in contact with exposure.

(2) *Elements on the wafer lower surface in contact with the stage*. The major heat source comes from the energy, q_s, taken away by the stage from the bottom of wafer, and the heat load produced is

$$\{F_t\} = \int\int_A q_s\{N\}\,dA = -\frac{k + k_s}{2\Delta L}\int\int_A \{N\}^T\{\Delta T\}\,dA, \tag{10}$$

where the thermal energy transferred to the stage per unit area, q_s, is

$$q_s = -\frac{k + k_s}{2}\frac{\Delta T}{\Delta L}$$

in this paper [13], k is the heat transfer coefficient of the wafer, k_s is the heat transfer coefficient of stage, ΔT is the difference in surface temperature between wafer and stage and ΔL is the vertical distance between the wafer and the element mass center on the stage contact face. The negative sign denotes that the heat source is released by wafer. The parameters used in this simulations are $k = 156$ w/m K, $k_s = 14$ w/m K and $\Delta L = 5.3$ cm [6]. The heat transfer of the contact between wafer and stage is treated as a boundary heat source for the sake of simplification. It is not necessary to calculate the temperature of the elements on the stage contact face and the temperature of the wafer bottom calculated at the previous time increment is used as the temperature of the stage contact face at the next time increment so as to derive the temperature difference, ΔT.

(3) *Elements on the wafer upper surface in the non-exposure region and on the wafer outer edge*. It is assumed that there is no external heat source or air thermal convection. Thus, the heat load produced is

$$\{F_t\} = 0. \tag{11}$$

3.2. Assumptions of material and exposure conditions

Table 1 shows the simulation parameters and exposure conditions assumed in this paper [1,8]. Th energy used in this simulation represents the value absorbed by the wafer, but not the heat source produced from the stepper. It also neglects the amount of the energy absorbed by photoresist coated on the wafer surface for the assumed four choices of exposure energy.

4. Results and discussions

In the following, we discuss the simulated results in four parts. It is including the effect of variation in finite element conditions on the analytical results, the transient behavior of thermal deformation of single exposure points during the exposure process, the effect of different orientations and intervals of the exposure locations of neighboring exposure regions and the variation of wafer deformation from absorbing the exposure energy.

4.1. Effect of grid density and time increment

Table 2 compares the temperature difference after wafer exposure derived from different grid densities. The source of data listed in the table come from the assumptions of a 17×17 mm^2 exposure field at the center point of the wafer a 500 mJ/cm^2 energy source, and a time increment of 0.01 s. The simulation results indicate that the highest temperature is at the center of the wafer. The distribution of temperature gradually decreases, as it gets further away from the center of the wafer along the *X*-axis. If the grid unilateral length is 8.5 mm, the temperature at the center of the exposure field is 296.253 K, while that at 25.5 mm from the field center 295.311 K. It is obvious from the trend of changes in the above data that when the grid unilateral length shrinks to 2.125 mm, the finite element analysis results already approximate stability.

Table 3 compares the difference in wafer temperature derived under different time increments. The grid unilateral length is constantly 4.25 mm. There are five different time increments adopted. The rest of the simulation conditions are the same as those in Table 2. If the time increment is 0.1 s, the temperature rises of the center point of wafer from the constant temperature of 295–296.192 K undergoes the exposure energy of

Table 1
Simulation parameters and exposure conditions [1,8]

Simulation parameters	
Wafer diameter	150 mm
Wafer thickness	0.6 mm
Wafer density, ρ	2330 kg/m^3
Thermal expansion coefficient	2.56×10^{-6}/K
Specific heat, c	761 J/kg K
Young's modulus, E	130 GPa
Poisson's ratio, v	0.28
Exposure conditions	
Wafer initial temperature	295 K
Area of each exposure	17×17 mm^2
Time of each exposure	Four choices of 0.6, 0.8, 1.0 and 1.2 s
Interval of exposure time	Four choices of 0.2, 0.3, 0.4 and 0.5 s
Interval of exposure locations	Three choices of the width of 1, 2 and 3 fields
Energy of each exposure	Four choices of 300, 400, 500 and 600 mJ/cm^2

Table 2
Comparison of wafer temperatures derived under different grid densities at constant time increment (0.01 s)

Distance from the center of exposure field (mm)	Grid unilateral length (mm)			
	8.5	4.25	2.125	1.0625
0.00	296.253	296.950	297.180	297.198
4.25	–	296.806	296.995	297.010
8.50	295.968	296.330	296.394	296.396
12.75	–	295.801	295.738	295.728
17.00	295.536	295.462	295.369	295.358
21.25	–	295.255	295.172	295.165
25.50	295.311	295.136	295.074	295.071

Unit of temperature: K.

Table 3
Comparison of wafer temperatures derived under different time increments at constant grid unilateral length (4.25 mm)

Distance from the center of exposure field (mm)	Variation in time increment (s)				
	0.1	0.01	0.005	0.001	0.0005
0.00	296.192	296.950	297.002	297.067	297.080
4.25	296.093	296.806	296.848	296.914	296.931
8.50	295.734	296.330	296.377	296.430	296.440
12.75	295.358	295.801	295.846	295.885	295.891
17.00	295.167	295.462	295.495	295.526	295.531
21.25	295.076	295.255	295.279	295.300	295.304
25.50	295.035	295.136	295.151	295.165	295.168

Unit of temperature: K.

500 mJ/cm^2. The temperature at 25.5 mm from the center point rises to 295.035 K. If the time increment is 0.01 s, the simulation results are fully identical with those listed in Table 2 under the grid unilateral length of 4.25 mm. The temperatures at the wafer center point and 25.5 mm away are 296.950 and 295.136 K, respectively. We can see from Table 3 that the time increment of 0.01 s already produces satisfactory convergence. The simulation results become more stable as the time increment decreases to smaller than 0.01 s.

As the simulation grid density increases, the temperature distribution derived from the wafer's center location rises. When the simulation time increment shrinks, the analysis results of the transient distribution of wafer temperature also approach stability. Under the considerations of computation precision and CPU time, the following simulations were conducted under the conditions of the time increment of 0.01 s and the unilateral grid length of 2.125 mm.

4.2. *Transient thermal deformation of single image field exposure*

The transient behaviors of changes in wafer shape and thermal stress distribution during the exposure process are the focus in this section. The input conditions of our simulation are as follows: the exposure time of 1.0 s (total exposure energy of 500 mJ/cm^2), exposure area of 17×17 mm^2 and the exposure location at the center of the wafer, i.e. point zero on the coordinate.

The temperature of various nodes at any time during wafer exposure can be derived from Eq. (2). The temperature can then be incorporated into Eq. (3) to obtain the displacement of various nodes. Fig. 3 shows the variation of wafer thickness due to thermal expansion during the process exposure. Given an exposure time of 0.1 s, the thickness at the center of the exposure field expanded 0.75 nm, while that at 8.5 mm away from the

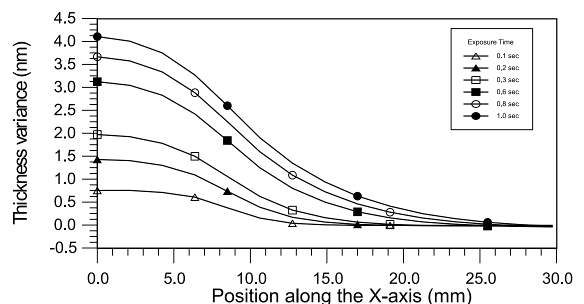

Fig. 3. Variation in wafer thickness change as a result of thermal expansion during exposure.

center expanded 0.375 nm, producing a height difference of 0.375 nm between the two locations. While an exposure time of 1.0 s, produced a height difference of 1.5 nm between the two locations, which is four times that under the exposure time of 0.1 s. In other words, after an increase in the exposure energy, the difference in height between the field center and boundary areas of the entire exposure field area grows. As a result, the depths of focus from projecting the mask pattern onto the wafer surface become inconsistent, which can easily causes blurring in part of the patterns.

Fig. 4 shows the horizontal displacement at different locations along the *X*-axis as a result of wafer thermal expansion during the exposure progress. Since the simulation conditions position the exposure point right on the wafer center, the thermal expansion moves horizontally to both sides, symmetrical with the wafer center. Hence, the displacement of the center point in the *X*-direction is zero. Restricted, the deformation can only expand in height. The displacement in the *X*-direction increases as the distance from the center point increases. For example, for an exposure time of 0.1 s, the displacement in the *X*-direction shows an almost linear increase from the center point to 10 mm away, reaching the maximum displacement of 5 nm. It experiences a slow decline after passing the 10 mm mark. This is because a smaller and smaller amount of energy is delivered to this location. In addition, the area surrounding the center point becomes larger as the distance from the point increases. Part of the deformation is absorbed by the *Y*-axis direction perpendicular to the *X*-axis direction. The above phenomenon is the same for the conditions between the exposure time of 0.1 and 1.0 s. However, after the exposure time exceeds 1.0 s, the maximum displacement grows from the 5 nm under 1.0 s to 30 nm, which occurs around 15 mm away from the field center. Considerable displacements still occur after the distance exceeds 15 mm. This is because the majority of the energy has been transmitted to the entire wafer through heat transfer.

As the exposure time reaches 1.0 s and the exposure is terminated, the wafer moves without any external energy being added to the wafer and some of the heat is transferred and dissipated through the stage in contact with the back surface of wafer. Fig. 5 shows the variation of wafer thickness change when the heat continues to dissipate at the end of the exposure. The thickness at the center of the exposure field increases 4.1 nm at the instant of the exposure termination, but decreases 2.1 nm, 0.5 s after the end of exposure, producing a difference of 2 nm. The thickness change shows a slight increase in areas beyond 14 mm away from the field center. This is caused by the gradual transmission of the exposure energy to areas beyond the exposure region. However, the maximum change does not exceed 0.2 nm and the extent of the decrease is far smaller than that at the field center.

Fig. 6 shows the horizontal displacement at different locations along the *X*-axis as the wafer continues to dissipate heat at the end of the exposure. At 0.5 s after the exposure, the maximum displacement along the *X*-axis direction drops from the original value of 32 nm at the instant of exposure termination to 25 nm. The location of the maximum displacement also moves from 15 to 22 mm from the field center. Another phenomenon

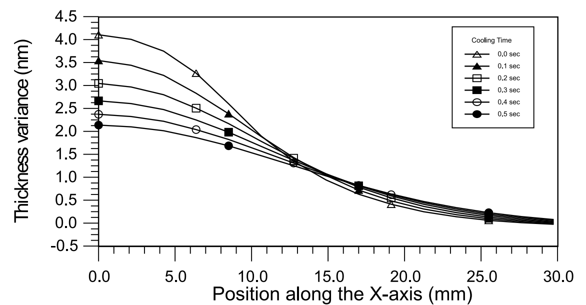

Fig. 5. Variation in wafer thickness change at different times after the termination of exposure.

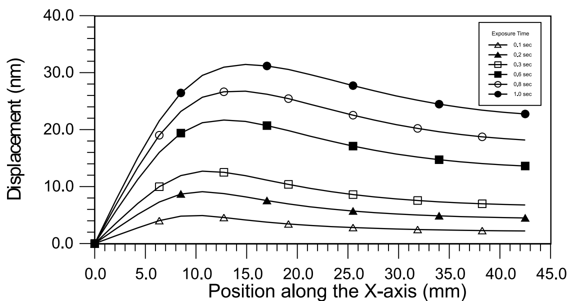

Fig. 4. Variation in horizontal displacement at different locations along the *X*-axis as a result of thermal expansion during exposure.

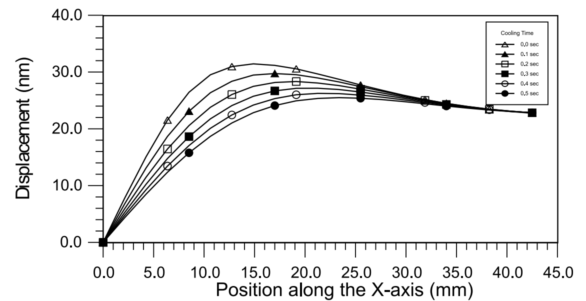

Fig. 6. Variation in horizontal displacement at different locations along the *X*-axis at different times after the termination of exposure.

shown in Fig. 6 occurs in the region beyond 34 mm from the field center. There is almost no variation in the displacement in the X-axis direction between the end of the exposure and 0.5 s afterwards. This is due to the insufficient time for transmission and dissipation and that the heat source transmitted from the exposure field center is very close to the energy lost from the transmission and dissipation at the back of wafer.

Fig. 7 shows the distribution of wafer thermal stress during exposure. The simulated exposure area is a square measuring 17×17 mm^2 and the exposure time is between 0.1 and 1.0 s. Fig. 7(a) shows the distribution of normal stress in the X-axis direction, σ_{xx}. For an exposure time of 0.1 s, the stress near the exposure center point, σ_{xx}, is around -65 kPa, the negative value indicating a compressive stress. The compressive stress is caused by higher temperature in the wafer exposure region compared to the peripheral regions. As the exposure time reaches 1.0 s, the stress near the center point of exposure area, σ_{xx}, increases to around -325 kPa. The stress gradually decreases as its distance from the exposure center increases. After the distance exceeds 37.5 mm from the exposure center, stress is hardly affected by the length of exposure time, and has a value under -10 kPa in all cases. In other words, in areas beyond 37.5 mm from the exposure center, the stress produced by exposure energy, σ_{xx}, can be ignored. Fig. 7(b) shows the distribution of normal stress in the Y-axis direction, σ_{yy}, which shares similar variation of stress near the exposure center point as σ_{xx}. However, dramatic changes are seen near 8.5 mm from the exposure center. Stress σ_{yy} becomes a tensile stress beyond 12.5 mm from the exposure center. This is because the exposure area is a square. After leaving the exposure region (8.5 mm from the exposure center) there is no heat source coming from the Y-axis direction at locations along the X-axis. The material in the Y-axis direction tends to be pulled toward the X-axis direction due to squeezing by thermal expansion. Thus, the stress σ_{yy} gradually turns from a compressive stress to a tensile stress. After the distance exceeds 37.5 mm from the exposure center, the stress σ_{yy} remains at approximately 70 kPa if the exposure time reaches 1.0 s.

If we use the equivalent stress, σ_e, in Eq. (5) to express the stress of various nodes of the wafer, the stress distribution of the wafer during the entire exposure process can be explained in Fig. 8. As the exposure time reaches 0.1 s, the stress distribution within the exposure region drops from 60 kPa near the center point to 45 kPa at the edge of the exposure region. After the distance exceeds 15 mm from the exposure center, lines of constant stress appear in concentric circles with the exposure center point as the center of circles. The stress values gradually decreases further away from the exposure center. In areas beyond 35 mm from the exposure center, the stress is smaller than 10 kPa. As the exposure time reaches 1.0 s, the accumulated exposure energy of 500 mJ/cm^2, the stress at the boundary of exposure region is close to 210 kPa, while that near the exposure center reaches 340 kPa. Even in regions beyond 35 mm from the exposure center, the stress values remains at 90 kPa and Cartesian coordinates are an acceptable approximation for the circular wafer.

From simulations of the transient behavior of single image field exposure, once exposure energy enters wafer, the wafer shape changes as a result of the continuous changes in temperature, regardless of the continuation or termination of exposure. Tensile stress and compressive stress occur near the exposure region become and more pronounced as the level of exposure energy increases.

4.3. Effect of thermal interactions between neighboring exposure regions

Fig. 9 shows the few options of neighboring exposure locations. In Fig. 9(a), after the image field exposure of the first exposure location is completed, the interval of

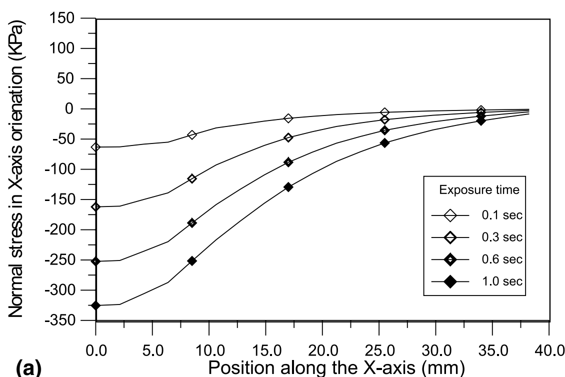

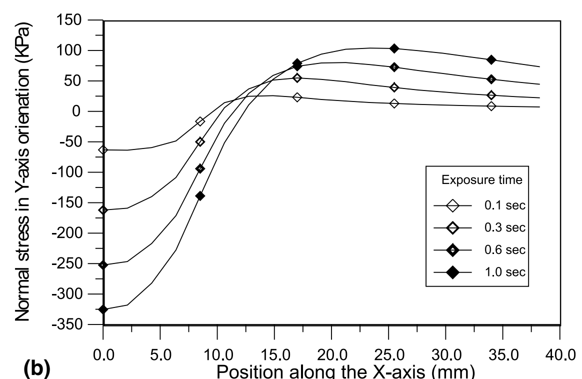

Fig. 7. Variation of wafer stress horizontal displacement at different locations along the X-axis during the progress of exposure: (a) distribution of the σ_{xx}; (b) distribution of the σ_{yy}.

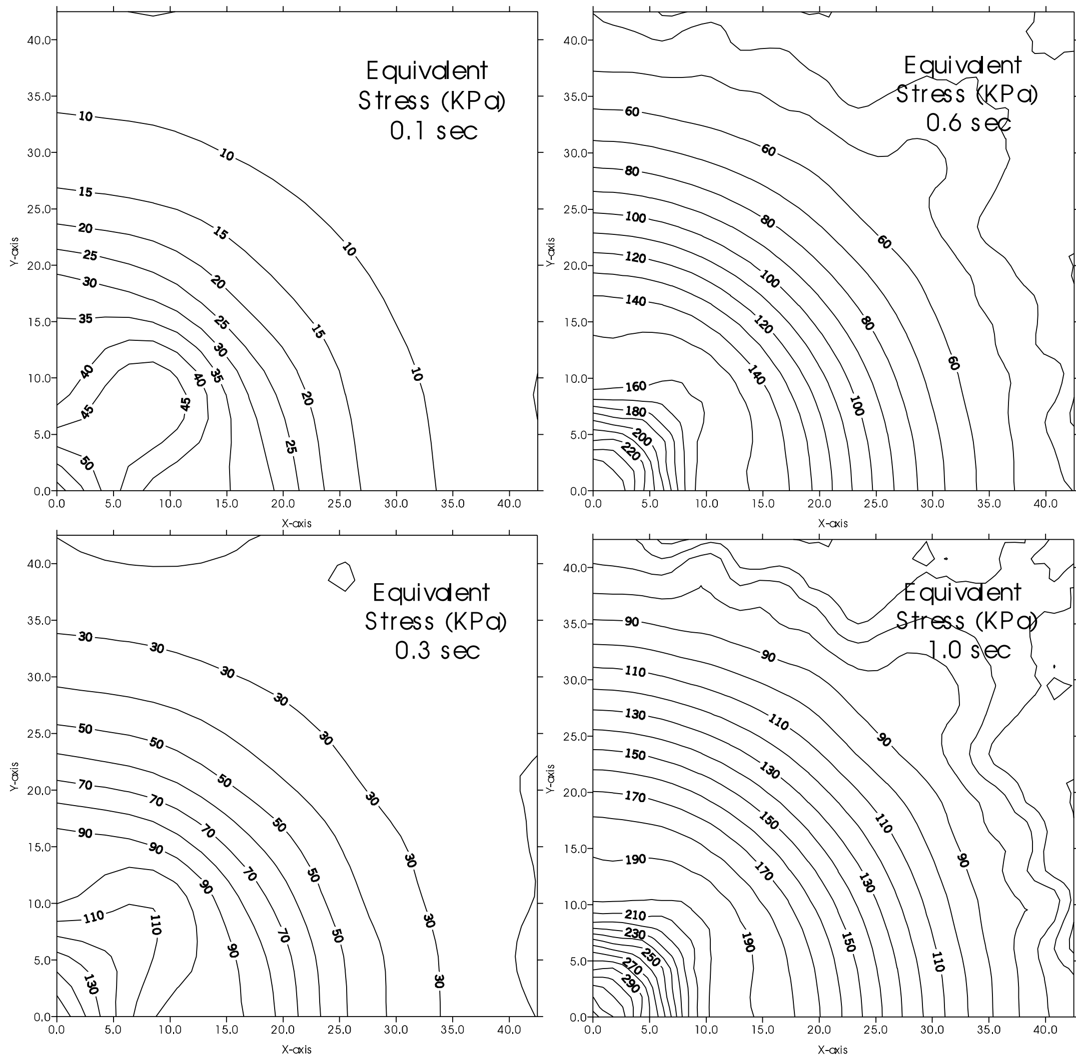

Fig. 8. Variation of wafer stress under different exposure time intervals.

one image field wide along the X-axis is chosen between the first and second exposure locations. The distance between the centers of two exposure fields is exactly one image field wide, which means that the left edge of the second exposure field is tightly linked to the right edge of the first exposure field. In Fig. 9(b), after the image field exposure of the first exposure location is completed, exposure of the second exposure field is conducted at a distance of one image field wide away in the 45°-direction of the X-axis. In other words, the center of the second exposure field is at a distance of one image field wide from the center of the first exposure field in both the directions of the X-axis and Y-axis. This suggests that the lower left corner of the second exposure field is connected to the upper right corner of the first exposure field. Therefore, the actual straight distance of exposure displacement shown in Fig. 9(b) is exactly 1.414 times of that shown in Fig. 9(a).

Let the first image field absorb 500 mJ/cm^2 of exposure energy and then conduct the exposure of the second image field after a lapse of 0.3 s. If the displacement path of the second image field adopts the pattern shown in Fig. 9(a), then the displacement deformation of the second image field, as shown in Fig. 10(a), will be obtained. The fine solid line in the figure denotes the image location during the exposure of the second image field, that is, the image location of the pattern projection on the wafer from the mask without considering the issue of deformation of the wafer. The wide solid line shows the actual displaced location due to the thermal expansion and deformation sustained by wafer. Here, we must note that the displacement shown

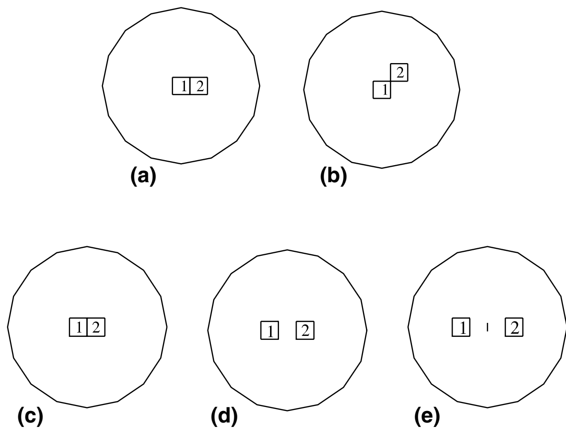

Fig. 9. Location orientations and interval orientations between neighboring exposure locations: (a) along the X-direction; (b) along the 45°-direction; (c) one field space; (d) two fields space; (e) three fields space.

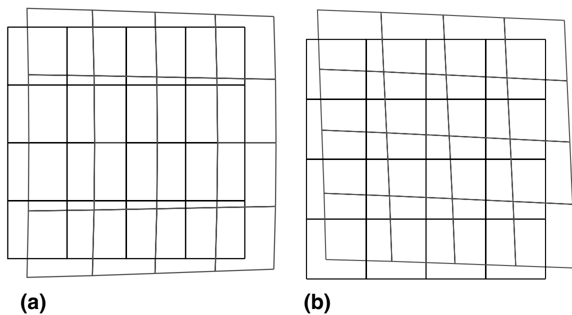

Fig. 10. Image field deformation as a result of different orientations of neighboring exposure locations: (a) along the X-axis direction; (b) along the 45°-direction.

in the figure has been magnified several hundred times for the purpose of distinguishing characteristics of the pattern variation. In reality, the maximum value of displacement is around 100 nm. Since the center of image field is located on the X-axis, the deformation of the image field is symmetrical to the X-axis. The original image field location of the wafer clearly tilts to the right. This is because the wafer sustains thermal expansion and expands outward. Looking closely at the figure, we can see that the entire image field has been magnified in addition to the parallel displacement of images and that the percentage of magnification is not equal between the left and right sides or the upper and lower sides. This means that the temperature on the left side of the image field is higher than that on the right. In addition, the entire image field is slightly bent and symmetrical to X-axis. Because here has a higher percentage of non-exposure regions at the corners of the image field and the rate of energy transfer is faster, the amount of expansion at the corners of the image field is slightly smaller than that at the locations on the axial line. If the displacement path of the second image field adopts the model shown in Fig. 9(b), then the displacement deformation of the image field is shown in Fig. 10(b). The figure shows that the deformation happens to be symmetrical to the 45°-line. Another distinctive feature in Fig. 10(b) is the rotating orthogonal deformation. This is because the level of energy transmission of the square image field in the X-axis and Y-axis directions falls behind that in the 45°-direction. There is also a less obvious phenomenon in this figure in that the pattern at the lower left corner of the image field is slightly magnified, while that at the upper right corner shrinks relatively. Based on the above analyses, we may infer that different exposure paths result in completely different deformation characteristics. These deformations all result from the expansion deformation of the wafer after absorbing heat source during the exposure process. But similar results [14,15] can be obtained from matching the systemic error parameters during the focusing of the stepper and wafer movement. This phenomenon signifies that the overlay error caused by thermal deformation can be implicitly contained in systemic error parameters. That is, proper corrective values of error parameters can be derived from the overlay analytical model to improve the overlay error.

Next, we consider the issue of intervals between exposure locations. Fig. 9(c)–(e) show the situations of three different intervals between exposure locations, where the number 1 denotes the location of the first exposure and the number 2 that of the second exposure. These exposures are symmetrical to the zero point of the coordinate at equal distances. The interval distance defined in this paper refers to the straight distance between the center point locations of the two neighboring exposure fields. Thus, for the distance of one image field defined in Fig. 9(c), the location of the second exposure is actually closely connected to that of the first exposure. As for the distance of the two image fields as defined, the shortest distance between the boundaries of two image fields is, in fact, only one image field wide. The same applies in the definitions for intervals of other fields.

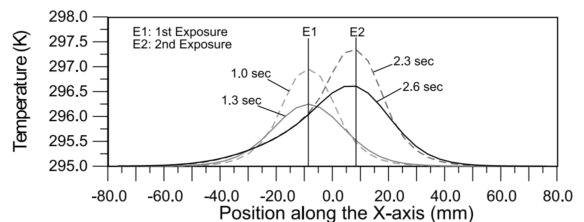

Fig. 11. Distribution of wafer transient temperatures when the interval of neighboring exposure locations is one image field wide.

Fig. 11 shows the simulated distribution of wafer temperature using an interval of one image field wide between neighboring exposure regions shown in Fig. 9(c). The exposure energy for each exposure field is 500 $\mathrm{mJ/cm^2}$ and the exposure time interval between two fields is 0.3 s. The first curve (1.0 s) in the figure denotes the distribution curve of wafer temperature along the X-axis at the instant right after the end of the first exposure. The curve shows a maximum temperature of 297 K at −8.5 mm on the X-axis, which is at the field center of the first exposure. The second curve (1.3 s) denotes the distribution of temperature right before the beginning of the second exposure, that is, 0.3 s after the end of exposure. The maximum temperature is around 296.2 K. The third curve (2.3 s) denotes the distribution of the temperature at the instant right after the end of the second exposure. The distance between the two exposure center locations is one image field wide and the maximum temperature is around 297.4 K, which occurs at 8.5 mm on the X-axis. This is the field center of the second exposure. The fourth curve (2.6 s) denotes the distribution of wafer temperature 0.3 s after the end of second exposure, with the maximum temperature 296.7 K. This curve also represents the distribution of wafer temperature right before it undergoes the third exposure. The figure shows that the wafer temperature at the second exposure is significantly higher than that at the first exposure.

Fig. 12 compares the variation of wafer thickness change 0.3 s after the end of the second exposure. The exposure sequence is shown in Fig. 11 and the intervals between the locations of neighboring exposure fields are shown in Figs. 9(c)–(e), which include the distances from one to five image field wide. As the interval between exposure fields change from one field to two or three fields wide, the maximum thickness change decreases from 3.1 to 2.6 and 2.3 nm, respectively. However, when the interval is set at four or five fields wide, the maximum thickness change does not show any significant decrease.

The above analyses indicate that different exposure paths produce different characteristics in the variation of patterns. As long as the distance between the field center locations of two neighboring exposure regions exceeds the straight distance equal to three image fields wide, changes in the thickness change approaches stability and the effect of interactions between neighboring exposure regions can be significant reduced.

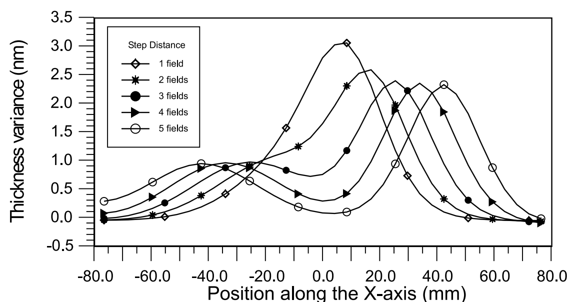

Fig. 12. Variation of wafer thickness change along the X-axis direction under different exposure location intervals.

4.4. Accumulated energy changes during continuous exposure

Fig. 13 shows the three options adopted in the simulation of exposure sequence in this paper. The symbols represent the same meaning as those in Fig. 9. The effect of changes in exposure energy on the wafer thickness under continuous exposure will be considered first. When the model of single field width as shown in Fig. 13(a) is adopted with four options of the energy level for each exposure, namely 300, 400, 500 and 600 $\mathrm{mJ/cm^2}$, and the time interval of neighboring exposure fields set at 0.3 s, the results shown in Fig. 14 are obtained. The figure shows the variation of wafer thickness change along the X-axis direction at 0.3 s after the end of the third exposure, which is under continuous exposure at four different levels of exposure energy. As shown in the figure, given the exposure energy of 300 $\mathrm{mJ/cm^2}$, the thickness change at the third exposure field center is 2.3 nm. As the exposure energy increases to 400, 500 and 600 $\mathrm{mJ/cm^2}$, the thickness at the above location rises to 2.8, 3.2 and 3.7 nm, respectively. The thickness at other

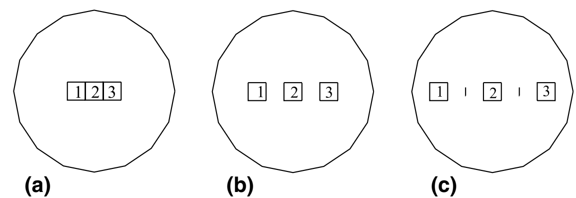

Fig. 13. Arrangement of exposure locations during continuous exposure: (a) one field space; (b) two fields space; (c) three fields space.

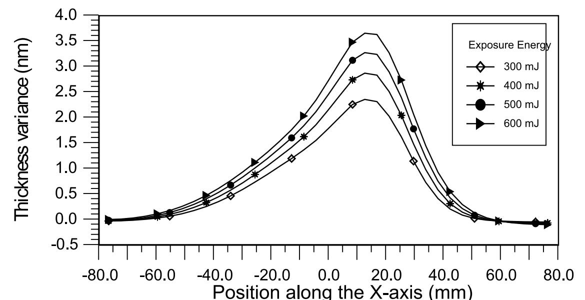

Fig. 14. Variation of wafer thickness change along the X-axis direction under different levels of exposure energy.

locations also increases as a result of increase in exposure energy, though not as much as that experienced at the center location.

The effect of different exposure time intervals on the distribution of wafer temperature and change in thickness is discussed next. Let the energy for each exposure remain constant at 500 mJ/cm^2. The exposure sequence and interval are as shown in Fig. 13(a), that is the centers of two neighboring exposure fields are one image field apart from each other. The intervals of exposure time between two neighboring image fields are set at 0.2, 0.3, 0.4 and 0.5 s. Similar to Fig. 14, the distribution of wafer thickness 0.3 s after the end of the third exposure is used to compare the effects of four different exposure time intervals. The results are shown in Fig. 15. As the exposure time interval increases gradually from 0.2 to 0.5 s, the wafer thickness increment at the third exposure center location drops from 3.7 to 2.8 nm. That is, the thickness change at the field center decreases as the exposure time interval lengthens. However, there is hardly any effect from the changes in exposure time interval at 34 mm from the wafer center, the center of image field at the fourth exposure.

Fig. 16 shows the variation of wafer thickness change at 0.3 s after the end of the third exposure along the *X*-axis direction under continuous exposure. Three models of exposure location interval are shown in Figs. 13(a)–(c) under the sequence of three image fields one, two and three image fields apart, respectively; a constant energy of 500 mJ/cm^2 at each exposure and a constant exposure time interval of 0.3 s. When the interval between two exposure center locations is one, two and three image fields, the corresponding thickness change at the third exposure center location drops to 3.3 to 2.5 or 2.2. A comparison between Figs. 15 and 16 indicates that widening the interval between exposure locations is more effective in improving the distribution of wafer thickness change than extending the exposure time interval of image fields. That is, the accumulation of energy during continuous exposure becomes more pronounced as the energy for each exposure increases.

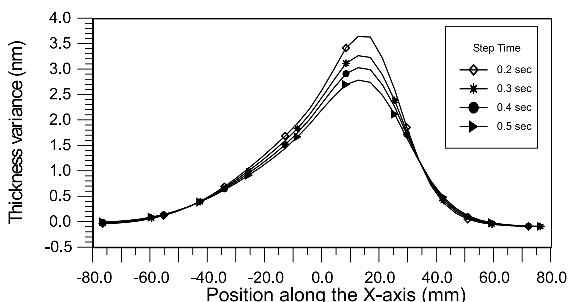

Fig. 15. Variation of wafer thickness change along the *X*-axis direction under different exposure time intervals.

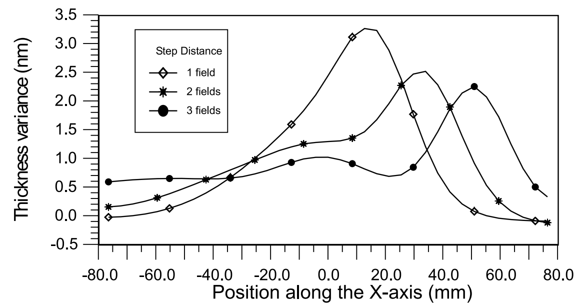

Fig. 16. Variation of wafer thickness change along the *X*-axis direction under different exposure location intervals.

5. Conclusion

The 3-D finite element model for analyzing the transient thermal elastic behavior of the wafer during exposure was established in this paper. The objective was to study the effect of different exposure conditions on the distribution of wafer temperature, thermal deformation, and stress conditions during exposure. Simulation results indicate that once exposure energy enters the wafer, the wafer shape changes as a result of the continuous changes in temperature, regardless of the continuation or termination of exposure. Tensile and compressive stresses occur near the exposure region and become more pronounced as the level of exposure energy increases.

Different exposure paths produced different characteristics of pattern deformation. Under the conditions assumed in this paper, widening the interval of exposure locations has a greater impact in improving the thermal deformation characteristics of the wafer than extending the interval of exposure time between the image fields. As long as the distance between the field center locations of two neighboring exposure regions exceeds the straight distance equal to the width of three image fields wide, the interacting thermal effect during wafer exposure can be ignored. Because exposure conditions vary with different requirements in the process, there is no single rule to get the best solution. Thus, the physical phenomenon discussed in this paper can serve as a supporting reference tool for engineers in planning exposure paths, and the simulation model can serve as an analysis tool to understand the behavior during the exposure process.

References

[1] T. Saito, S. Sakamoto, K. Okuma, H. Fukumoto, Y. Okuda, Mask overlay scaling error caused by exposure energy using a stepper, SPIE, Integrated Circuit Metrology, Inspection, and Process Control VII 1926 (1993) 440–449.

[2] R.E. Gegenwarth, F.P. Laming, Effect of plastic deformation of silicon wafers on overlay, Proceedings of the SPIE, Semiconductor Microlithography II, 100 (1977) 66–73.
[3] L.D. Yau, Process-induced distortion in sillicon wafers, IEEE Trans. Electron Devices ED-26 (9) (1979) 1299–1305.
[4] J.H. Lau, Thermoelastic solutions for a finite substrate with an electronic device, Trans. ASME J. Electronic Packaging 113 (1991) 84–88.
[5] J.H. Lau, Thermoelastic solutions for a semi-infinite substrate with a powered electronic device, Trans. ASME J. Electronic Packaging 114 (1992) 353–358.
[6] E. Haytcher, R. Engelstad, Finite element analysis of dynamic thermal distortions of an X-ray mask for synchrotron radiation lithography, Proc. SPIE 1671 (1992) 347–356.
[7] Y.-L. Shen, S. Suresh, I.A. Blech, Stresses, curvatures, and shape changes arising from patterned lines of silicon wafers, J. Appl. Phys. 80 (3) (1996) 1388–1398.
[8] J. Lee, A.S. Mack, Finite element simulation of a stress history during the manufacturing process of thin film stacks in VLSI structures, IEEE Trans. Semicond. Manuf. 11 (3) (1998) 458–464.
[9] J.F. Buller, M.M. Farahani, S. Garg, Manufacturing issues related to RTP induced overlay errors in a global alignment stepper technology, IEEE Trans. Semicond. Manuf. 9 (1) (1996) 108–114.
[10] J.P. Hebb, K.F. Jensen, The effect of patterns on thermal stress during rapid thermal proceeding of silicon wafers, IEEE Trans. Semicond. Manuf. 11 (1) (1998) 99–107.
[11] J.-M. Dilhac, N. Nolhier, C. Ganibal, C. Zanchi, Thermal modeling of a wafer in a rapid thermal processor, IEEE Trans. Semicond. Manuf. 8 (4) (1995) 432–439.
[12] K.H. Huebner, E.A. Thornton, The Finite Element Method for Engineers, Wiley, New York, 1995, pp. 284–295.
[13] Z.C. Lin, C.J. Lee, A coupled analysis of the thermo-elastic-plastic large deformation for upsetting process, J. Chinese Soc. Mech. Engrg. 10 (3) (1989) 197–209.
[14] Z.C. Lin, W.J. Wu, A study of improving overlay accuracy for a stepper in IC manufacture, Int. J. Adv. Manuf. Technol. 14 (1998) 835–847.
[15] Z.C. Lin, W.J. Wu, Multiple linear regression analysis of the overlay accuracy model, IEEE Trans. Semicond. Manuf. 12 (2) (1999) 229–237.